The Northeast Winter Monsoon over the Indian Subcontinent and Southeast Asia: Evolution, Interannual Variability, and Model Simulations

AGNIV SENGUPTA AND SUMANT NIGAM

Department of Atmospheric and Oceanic Science, University of Maryland, College Park, College Park, Maryland

ABSTRACT

The northeast monsoon (NEM) brings the bulk of annual rainfall to southeastern peninsular India, Sri Lanka, and the neighboring Southeast Asian countries. This October–December monsoon is referred to as the winter monsoon in this region. In contrast, the southwest summer monsoon brings bountiful rainfall to the Indo-Gangetic Plain. The winter monsoon region is objectively demarcated from analysis of the timing of peak monthly rainfall. Because of the region's complex terrain, in situ precipitation datasets are assessed using high-spatiotemporal-resolution Tropical Rainfall Measuring Mission (TRMM) rainfall estimates, prior to their use in monsoon evolution, variability, and trend analyses. The Global Precipitation Climatology Center's in situ analysis showed the least bias from TRMM.

El Niño–Southern Oscillation's (ENSO) impact on NEM rainfall is shown to be significant, leading to stronger NEM rainfall over southeastern peninsular India and Sri Lanka but diminished rainfall over Thailand, Vietnam, and the Philippines. The impact varies subseasonally, being weak in October and strong in November. The positive anomalies over peninsular India are generated by anomalous anticyclonic flow centered over the Bay of Bengal, which is forced by an El Niño–related reduction in deep convection over the Maritime Continent.

The historical twentieth-century climate simulations informing the Intergovernmental Panel on Climate Change's Fifth Assessment (IPCC-AR5) show varied deficiencies in the NEM rainfall distribution and a markedly weaker (and often unrealistic) ENSO–NEM rainfall relationship.

1. Introduction

Monsoons over South Asia are characterized by a southwest summer monsoon from June to September and a northeast monsoon (NEM) from October to December (OND). The boreal summer monsoon, which brings copious amounts of rainfall accounting for over 70% of the annual rainfall over India, has been more widely studied. However, southeastern peninsular India remains in the rain-shadow region of the Western Ghats, the orographic barrier along the west coast that shields the region from the moisture-laden southwest monsoon winds. The agricultural productivity in this region is largely dependent on the NEM rainfall, which supplies nearly 50% of the annual rainfall to southeastern peninsular India, Sri Lanka, and the neighboring seas (Kumar et al. 2007). The prospect of seasonal prediction along with its impacts on water resources and agriculture (the winter crops: Rabi in southern

India and Maha in Sri Lanka) warrants a closer look at the winter monsoon and its variability.

Despite its significant agricultural and economic importance, the NEM has been considerably understudied relative to its summer monsoon counterpart. The India Meteorological Department forecasting manual (Srinivasan and Ramamurthy 1973) provided a detailed description of the NEM. Dhar and Rakhecha (1983) studied monthly rainfall data for a 100-yr period (1877–1976) to investigate the association between the northeast and southwest monsoons over Tamil Nadu, India, and concluded that summer rainfall is negatively correlated with NEM rainfall. Matsumoto (1990) investigated variations in tropical wind fields and noted activation of the NEM during the end of October in the northern Indian Ocean sector. Singh and Sontakke (1999) examined the Indian postmonsoon rainfall features and its variability and attempted to extrapolate the future trend in rainfall fluctuations over a 10-yr period. Wang and LinHo (2002) noted a bimodal seasonal

Corresponding author: Agniv Sengupta, agnivs@umd.edu

distribution of rainfall over Sri Lanka and Indochina with rainfall maxima in October–November. The interannual variation of late-autumn rainfall over Vietnam was discussed by Chen et al. (2012). NEM also influences the eastern coast of the Philippines (Akasaka et al. 2007); however, its onset and interannual variation do not show prominent fluctuations like those of the summer rainy season (Akasaka 2010).

The El Niño–Southern Oscillation (ENSO) phenomenon is perhaps the most studied mode of interannual climate variability since Bjerknes (1969) linked El Niño SST anomalies with basinwide sea level pressure variations (Southern Oscillation; Walker 1923). Over India, El Niño events have been associated with below-normal summer monsoon rainfall (Sikka 1980; Rasmusson and Carpenter 1983; Pant and Kumar 1997; Kumar et al. 2007). El Niño's impact on the NEM is, however, the opposite (Sridharan and Muthuswamy 1990; Suppiah 1997; De and Mukhopadhyay 1999; Jayanthi and Govindachari 1999), that is, above-normal rainfall. Contrary to the robust ENSO–NEM rainfall link over South Asia, the relationship between ENSO and the East Asian winter monsoon (EAWM) undergoes low-frequency oscillation (Zhou et al. 2007) with a periodicity of about 50 years (He and Wang 2013).

ENSO is widely monitored using the Niño SST indices, for example, the Niño-3.4 index—the area-averaged SST anomaly in the equatorial central-eastern Pacific Ocean, computed, for example, using HadISST data (Rayner et al. 2003). The relationship between ENSO and the NEM has strengthened in the recent past (Zubair and Ropelewski 2006; Kumar et al. 2007), whereas the relationship between ENSO and the EAWM has weakened since the mid-1970s (Wang and He 2012). Wang et al. (2008) found that the Pacific decadal oscillation, whose negative phase leads to robust low-level temperature change over East Asia, modulates the ENSO–EAWM relationship. Sun et al. (2011) identified the Atlantic meridional overturning circulation as a potential driver of the abrupt changes in the EAWM from rainfall reconstruction over the past 60 000 years using grain-size records in northwestern China's Loess Plateau. In contrast, comparatively little is known about the decadal–multidecadal variability of the NEM over the Indian subcontinent and Southeast Asia.

Likewise, historical simulations and future projections of the South Asian summer monsoon rainfall have been analyzed in numerous studies: The simulations show the presence of large systematic biases in summer precipitation and evaporation over the Indian subcontinent and Indian Ocean (Bollasina and Nigam 2009), while the projections indicate a consistent increase in summer season rainfall (Endo and Kitoh 2016; Sharmila et al.

2015; Sengupta and Rajeevan 2013; Menon et al. 2013) but with weakening of the large-scale monsoon circulation (Sooraj et al. 2015). In contrast, there are few analyses of the NEM simulations and projections: Siew et al. (2014) evaluated 10 atmosphere–ocean general circulation model simulations over Southeast Asia and the Maritime Continent and found widespread biases across the region; a weaker relationship between regional rainfall and ENSO and thus reduced interannual variability was also noted. Parvathi et al. (2017) recently noted the weakening of winter monsoon winds over the Arabian Sea in the Intergovernmental Panel on Climate Change's Fifth Assessment (IPCC-AR5) climate projections, which was attributed to the reduction in the interhemispheric sea level pressure gradient. The projected change in the low-level winds to the east of the Indian Peninsula (i.e., over the southern Bay of Bengal), a key circulation element of the NEM, was not discussed.

This study is motivated by the evaluative opportunities presented by the lack of analyses of the NEM rainfall and circulation climatologies and their interannual variability, especially in the context of the IPCC-AR5 simulations and projections. Datasets and analysis method are discussed in section 2. Seasonal hydroclimate variability over the South and Southeast Asian continent is presented in section 3, including a harmonic analysis showing the annual mean and annual cycle of observed rainfall. The spatial distribution of the climatological OND rainfall, circulation, and related rainfall standard deviation is also described in section 3, followed by an intercomparison of in situ and satellite-based precipitation estimates. The rendition of seasonal hydroclimate variability over South and Southeast Asia in select IPCC-AR5 historical simulations is critiqued in section 4, followed by an evaluation of the models' skill in replicating the observed OND climatological rainfall distribution. ENSO's characteristic influence on the northeast monsoon in observations and historical climate simulations is described in section 5, which also investigates the influence mechanism. The linear trend in northeast monsoon hydroclimate—rainfall and low-level winds—is examined in section 6. Concluding remarks, including implications of this analysis for the potential prediction of winter monsoon rainfall and its hydroclimate impacts, follow in section 7.

2. Datasets and analysis method

a. Observed precipitation

Four different gridded rainfall datasets are used to investigate the OND NEM rainfall distribution, including seasonal and interannual variability, and the

TABLE 1. List of CMIP5 GCMs used in this study with their spatial resolution, available time period, and number of ensemble members [as in Nigam et al. (2017)]. Expansions of model names and modeling centers are available online (https://ametsoc.org/pubsacronymlist).

Model name	Modeling center	No. of realizations (ensemble size)	Spatial resolution (lon × lat)	Available time period
CCSM4	NCAR	6	$1.25° \times 0.942°$	1850–2005
GFDL CM3	NOAA GFDL	5	$2.5° \times 2.0°$	1860–2004
HadCM3	UKMO	9	$3.75° \times 2.5°$	1860–2005
HadGEM2-ES	UKMO	4	$1.875° \times 1.25°$	1860–2005
MPI-ESM-LR	MPI	3	$1.875° \times 1.865°$	1850–2005

influence of ENSO. The Climatic Research Unit (CRU) Time Series, version 4.00 (CRU-TS4.00; Harris et al. 2014), at $0.5° \times 0.5°$ resolution is high-resolution gridded data of month-by-month variation in climate, available online over the land points for the January 1901–December 2015 period (from https://crudata.uea.ac.uk/cru/data/hrg/cru_ts_4.00). The Global Precipitation Climatology Centre (GPCC; Schneider et al. 2014; Becker et al. 2013) Full Data Reanalysis, version 7, on a 0.5° continental grid (provided online by the Physical Sciences Division of the NOAA Earth System Research Laboratory; https://www.esrl.noaa.gov/psd/data/gridded/data.gpcc.html) is a quality-controlled monthly precipitation dataset derived from 67 200 stations worldwide for the January 1901–December 2013 period using the WMO Global Telecommunication System (GTS), synoptic weather reports (SYNOP), and monthly climate reports (CLIMAT).

The Asian Precipitation—Highly Resolved Observational Data Integration Toward Evaluation of Water Resources (APHRODITE; Yatagai et al. 2012), version 1101 (v1101), is a daily gridded precipitation dataset available online at $0.5° \times 0.5°$ resolution for the January 1951–December 2007 period (http://www.chikyu.ac.jp/precip/english/products.html). The monthly mean is computed from the daily APHRODITE precipitation data, which are available over land from a dense network of rain gauge data over Asia. Last, the joint United States–Japan Tropical Rainfall Measuring Mission (TRMM) satellite product 3B42, version 7 (3B42v7; Huffman et al. 2007, 2010), is available online at $0.25° \times 0.25°$ resolution over both the land and ocean for the period January 1998–present (with a 2-month latency) (https://disc2.gesdisc.eosdis.nasa.gov/data//TRMM_L3/TRMM_3B42_Daily.7/). The TRMM algorithm 3B42 produces merged (satellite rainfall estimates with gauge data) high-quality precipitation data and root-mean-square (RMS) precipitation error estimates on a 3-h temporal resolution in a global belt extending from 50°S to 50°N. The daily-accumulated precipitation product is generated from these 3-hourly merged precipitation estimates.

b. Observed winds and sea level pressure

The analysis draws on the National Centers for Environmental Prediction (NCEP) reanalysis (Kalnay et al. 1996) to characterize the circulation associated with the NEM, especially the 925-hPa winds and mean sea level pressure (MSLP). This dataset is a global retrospective analysis of atmospheric fields via recovery of land surface, ship, rawinsonde, pibal, aircraft, satellite, and other data, followed by quality controlling and data assimilation, available at monthly resolution on a $2.5° \times 2.5°$ global grid at 17 pressure levels from January 1949 (http://iridl.ldeo.columbia.edu/SOURCES/.NOAA/.NCEP-NCAR/.CDAS-1/.MONTHLY).

c. Observed diabatic heating and streamfunction

The European Centre for Medium-Range Weather Forecasts (ECMWF) interim reanalysis (ERA-Interim; Dee et al. 2011), a state-of-the-art global atmospheric reanalysis for the 1979–present period obtained from a four-dimensional variational data assimilation system, is used for diagnosis of diabatic heating and streamfunction. The heating diagnosis (N. Dai et al. 2018, unpublished manuscript) follows the strategy outlined in Chan and Nigam (2009); see also Nigam et al. (2000). The mass-weighted vertically averaged (surface–100 hPa) diabatic heating and 850-hPa streamfunction are analyzed in the context of the ENSO influence mechanism.

d. Historical climate simulations

Simulations of twentieth-century climate forced by historical greenhouse gas emissions, aerosol loadings, and solar activity are referred to as historical climate simulations (Taylor et al. 2012). Historical simulations of precipitation and SST from five CMIP5 models informing the IPCC-AR5 are analyzed in this study; pertinent features of the models are noted in Table 1. Models from the major climate modeling centers of the United States—the National Center for Atmospheric Research (NCAR) and NOAA's Geophysical Fluid Dynamics Laboratory (GFDL)—and Europe—the Met Office (UKMO) and the Max Planck Institute (MPI)—are investigated, as in Nigam et al. (2017).

e. Analysis method

The analysis domain is the Indian subcontinent and Southeast Asia (5°–40°N, 60.25°–123°E), and the analysis

is restricted to the post-International Geophysical Year (IGY) period (1958–present). The NEM extends from October to December, consistent with the India Meteorological Department's definition (http://www.imdchennai.gov.in/northeast_monsoon.htm); NEM plots are constructed by averaging the OND fields. Analysis of the IPCC-AR5 simulations and projections is based on each model's ensemble mean; the number of ensemble members is noted in Table 1.

The ENSO–NEM relationship is characterized from the temporally leading (OND) regressions of precipitation on the winter [December–February (DJF) averaged] Niño-3.4 SST index in the post-IGY period (1958–2013). Because ENSO SST anomalies are robust in boreal winter, using just the winter value of the Niño-3.4 SST index ensures robust tracking of ENSO variability. The Niño-3.4 SST index is constructed by areal averaging of the SST anomalies in the 5°S–5°N and 170°–120°W domain, using the "aave" function in the Grid Analysis and Display System (GrADS-2.1.a3) toolkit. In most figures, a nine-point smoother (the "smth9" function in GrADS) is applied to highlight the coherent, larger-scale spatial features.

The statistical significance of the regressions at the 95% level is evaluated through a two-tailed Student's t test using the original sample size. The t value from observations is calculated via the following formula: $t = r(n - 2)^{1/2}/(1 - r^2)^{1/2}$, where $n = N$ is the original sample size and r is the correlation at each grid point. The results were almost identical while using an effective sample size, $n = N_e$ [following the method of Quenouille (1952)], suggesting that serial correlation is not an issue for this analysis.

The statistical significance of a rainfall trend is computed as the ratio between its slope and standard error. Trends are considered to be statistically significant when the t value of observations computed using an effective sample size n_e from lag-1 autocorrelation of the residual time series $e(t)$ exceeds the critical t value at 95% level [following the adjusted standard error and adjusted degrees of freedom method (AdjSE + AdjDF); Santer et al. 2000].

3. Hydroclimate variability over South and Southeast Asia

a. Seasonal cycle

Precipitation and surface air temperature are the extensively monitored hydroclimate fields. The annual mean and annual cycle of observed precipitation from the GPCC (version 7; land-station based) and TRMM (3B42v7; satellite based, and thus for both land and ocean) data are displayed in Fig. 1. A harmonic analysis

(Wilks 2006) of the climatological monthly mean precipitation is performed to extract the annually varying component, which is displayed using vectors, with the length denoting the amplitude of the annual cycle and the direction indicating its peak phase, following Nigam and Ruiz-Barradas (2006). The rainfall annual mean is shown with superposed contours plotted at a 1.0 mm day^{-1} interval (Fig. 1). It is notably large (~7–8 mm day^{-1}) on the western coast (Konkan) and northeastern states of India, and over Bangladesh, Myanmar, and the Philippines; over southeast peninsular India and Sri Lanka, the annual-mean rainfall is 3–4 mm day^{-1}. On the other hand, rainfall is scanty (<2 mm day^{-1}) over northwestern India and central and southern Pakistan and moderate (3–4 mm day^{-1}) over eastern China. Over the oceans (see Fig. 1, lower panel), the rainfall annual mean is large (~6–8 mm day^{-1}) over the eastern Bay of Bengal along Bangladesh and Myanmar coastlines [in agreement with Shige et al. (2017)] and over the southeastern South China Sea.

The vectors in Fig. 1—their large amplitude and especially direction—succinctly capture the prominent seasonality (i.e., monsoonal nature) of rainfall over South and Southeastern Asia: The summer monsoon rainfall over India, Bangladesh, and the Indochina Peninsula peaks in July (blue vectors pointing northward), while the pre-mei-yu and mei-yu rainfall over eastern China peaks in late spring (blue arrows pointing northwestward). Also present in Fig. 1 are regions where rainfall peaks in late autumn and early winter (red arrows pointing east and southeastward); these regions, primarily confined to the eastern coasts, are far smaller in extent than the spring to summer monsoon rainfall region, which encompasses large swaths of the southern continent. Notable regions of peak early winter rainfall—the focus of this study—are southeastern peninsular India, Sri Lanka, and the east coasts of Thailand, Malaysia, Vietnam, and the Philippines. In the Indian subcontinent, the early winter rainfall is often referred to as the NEM, or just the winter monsoon; the "northeast" attribute comes from the prevailing surface northeasterlies, shown later in Fig. 2.

The TRMM precipitation that provides a rare view of the rainfall over tropical oceans is analyzed in the lower panel of Fig. 1. Harmonic analysis of the land–ocean rainfall shows that the NEM rainfall region is not just confined to peninsular India, Sri Lanka, and the east coast regions in Southeast Asia but expansive, extending over large sectors of the neighboring seas, for example, southwestern Bay of Bengal, north-equatorial Indian Ocean, and the western South China Sea. Minor discrepancies in vector magnitude and orientation between GPCC and TRMM annual cycles are found over remote
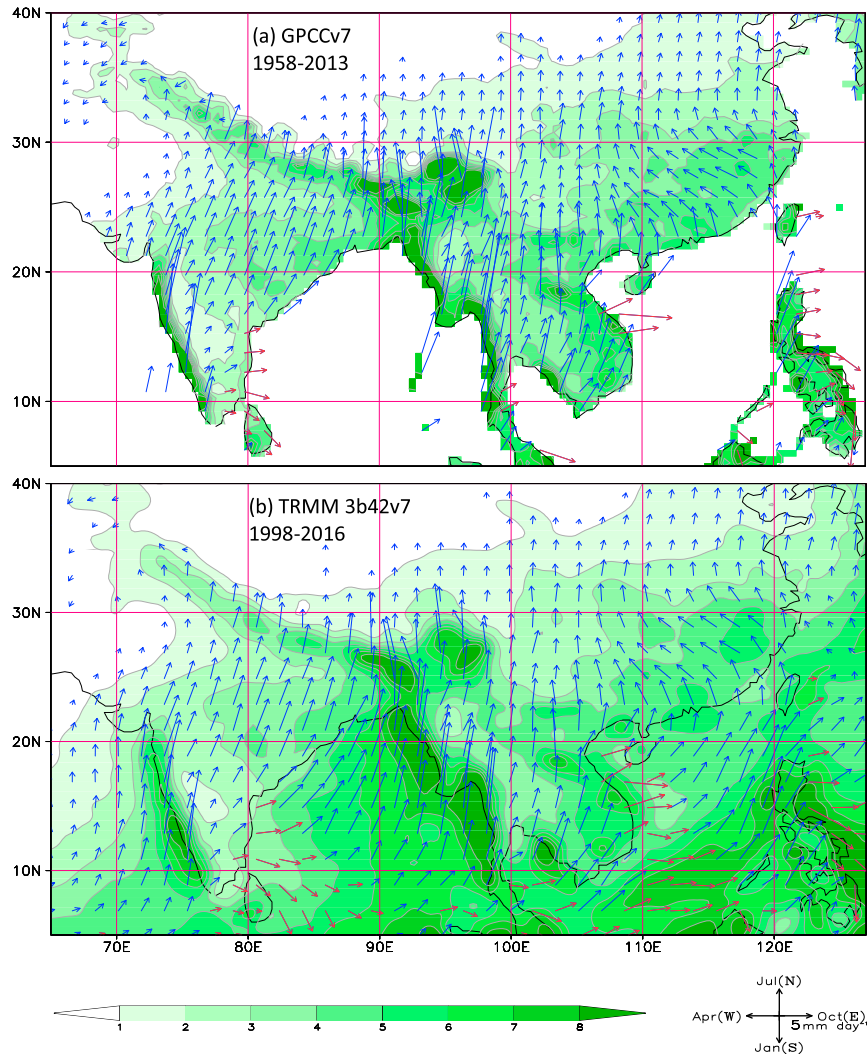
FIG. 1. Annual mean and annual cycle of rainfall for (a) GPCC, version 7 (1958–2013), and (b) TRMM, 3B42v7 (1998–2016). Vectors represent the annual cycle (first harmonic), and contours show the annual mean (mm day^{-1}). Vector scaling and the phase of the annual cycle are shown on the lower right; vectors pointing north indicate July as the maximum rainfall month, and so on. Vectors in red represent regions receiving winter monsoon rainfall during the OND season. The rainfall annual mean is contoured and shaded at 1.0 mm day^{-1} intervals. The amplitude threshold for plotting vectors is 0.75 mm day^{-1}. The plot in (b) is shown after four applications of smth9 in GrADS.

mountainous regions in the northeastern sector of the subcontinent (e.g., Bhutan, Assam, and Myanmar) and over the Western Ghats in peninsular India; some of the discrepancies result from the different climatology periods. Note, in some regions of India and Bangladesh, the amplitude of the annual cycle is larger than the annual mean, reflecting the presence of semiannual variability (originating from an extended dry season).

b. NEM rainfall and circulation

The spatial distribution of NEM rainfall and associated sea level pressure and low-level circulation is displayed at monthly resolution during October–January in Fig. 2. October is evidently the wettest month in the period, with rainfall progressively decreasing through January. Southeast peninsular India records more than 6.0 mm day^{-1} in October, 4.5 mm day^{-1} in November, and more than 1.5 mm day^{-1} in December; there is no significant rainfall in January. October rainfall is large also over Sri Lanka ($>$6.0 mm day^{-1}), Vietnam ($>$9.0 mm day^{-1}), the Philippines ($>$6.0 mm day^{-1}), Myanmar ($>$4.5 mm day^{-1}), Laos ($>$3.0 mm day^{-1}), Cambodia ($>$4.5 mm day^{-1}), and Thailand ($>$3.0 mm day^{-1}). Rainfall becomes more coastally confined as the winter monsoon
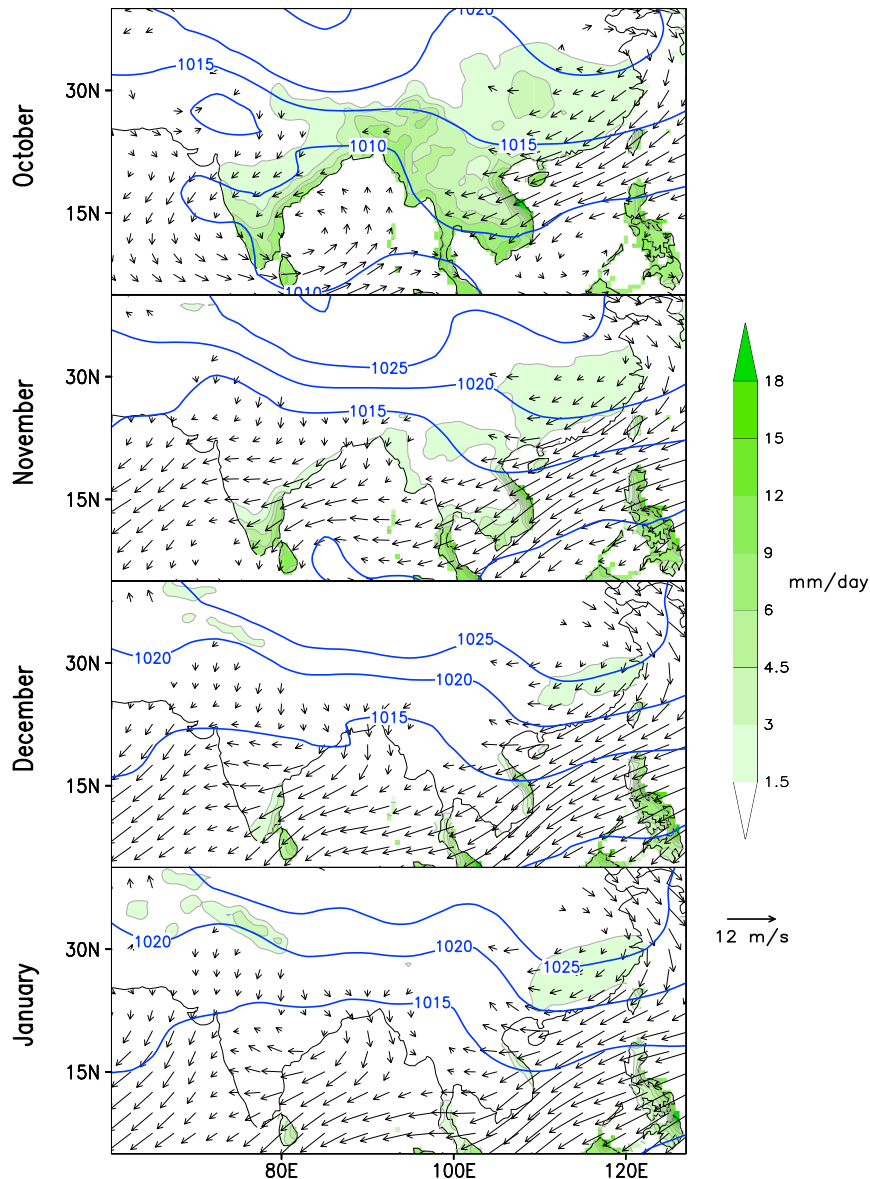
FIG. 2. Climatological rainfall (GPCC, version 7), 925-hPa vector winds, and MSLP (NCEP reanalysis) for the months of October, November, December, and January. The period of analysis is 1958–2013. The contour interval (CI) for rainfall is 1.5 mm day^{-1} for values of less than 6.0 mm day^{-1} and is 3.0 mm day^{-1} for higher values; the shading threshold is 1.5 mm day^{-1}. The threshold for plotting wind vectors is 1.0 m s^{-1}; SLP is contoured at 5 hPa. The rainfall field is displayed after one application of smth9.

season progresses, with the entire continent, except Sri Lanka and the Malay Peninsula, devoid of rainfall in January.

A salient feature of the seasonal circulation during the winter monsoon is the low-level northeasterly flow over the Indian subcontinent and Southeast Asia. Interestingly, in October—the wettest month of the monsoon—the onshore flow from the Bay of Bengal is easterly, with the northeasterlies confined to peninsular

India. This flow structure is, of course, consistent with the presence of a low pressure center over the southwestern Bay of Bengal (e.g., the 1010-hPa isobar in Fig. 2, top panel) and the associated cyclonic (counterclockwise) circulation. The advent of significant northeasterly winds (~5–8 m s^{-1}) over the Bay of Bengal in November (i.e., a month after their appearance over the South China Sea) reflects organization by the southern flank of the emerging continental-scale Siberian high;
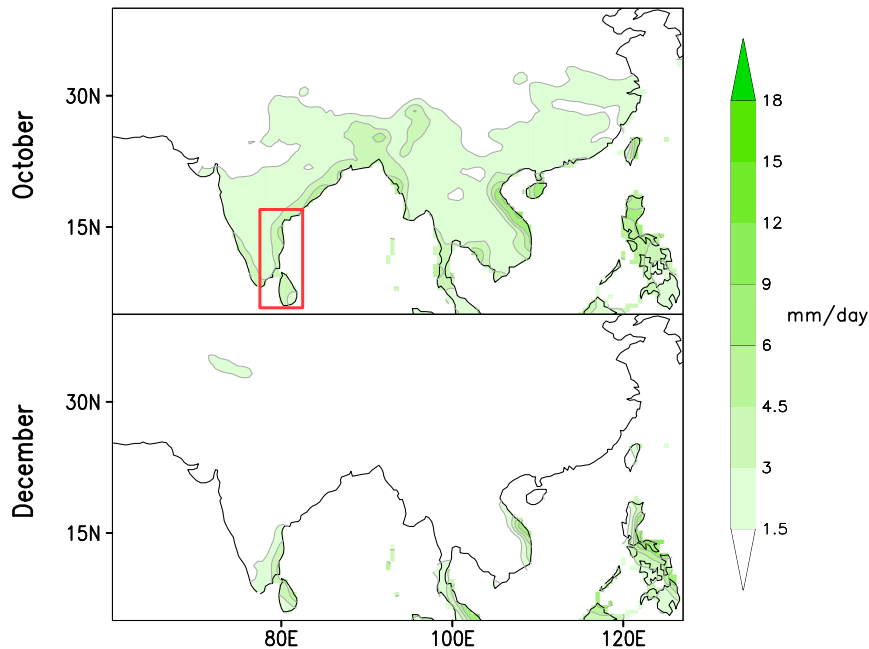
FIG. 3. The SD of rainfall (1958–2013) showing rainfall variability from the GPCC, version 7, dataset for the months of October and December. The CI is 1.5 mm day^{-1} for values of less than 6.0 mm day^{-1} and is 3.0 mm day^{-1} for higher values; the shading threshold is 1.5 mm day^{-1}. The fields are displayed after one application of smth9.

see the SLP distribution in Fig. 2.[1] The northeasterly flow remains firmly embedded in the region, at least until January, accounting for winter rainfall in the narrow onshore coastal regions. Over the South China and Philippine Seas, the northeasterly winds are established in October itself (i.e., earlier than the Bay of Bengal),[2] as part of the regional high-SLP feature over northern China. The northeasterlies bring impressive winter rains, especially over the eastern coasts of Vietnam and Thailand, and also over the Philippines, Laos, and Cambodia.

c. Interannual variability of NEM rainfall

The interannual variability of rainfall is assessed in Fig. 3 from the display of the rainfall standard deviation (SD) in October and December, the start and end months of the NEM season. In October, the SD over southeastern peninsular India and Sri Lanka is 1.5–4.5 mm day^{-1} against a climatology of ~6 mm day^{-1}, whereas the SD is >3 mm day^{-1} over Vietnam, where climatological rainfall is ~9 mm day^{-1}; the SD is large over the Philippines as well. The October rainfall SD is also large (>3 mm day^{-1}) over Bangladesh and north-eastern India, although this region is not an NEM region (cf. Fig. 1b). The December rainfall is seemingly less variable but not when viewed relative to its climatology; for example, SD over coastal peninsular India is 1.5–3.0 mm day^{-1} against a regional climatology of ~3 mm day^{-1}.

d. NEM rainfall in in situ and satellite-based precipitation analyses

The climatological OND rainfall is displayed over land and ocean in Fig. 4 using TRMM data, and the three gauge-based precipitation analyses commonly used to monitor rainfall over the Asian continent are compared with the satellite-based precipitation estimate; the climatology is based on the common 10-yr period (1998–2007)[3] of the four datasets. Although the

---

[1] October is the transition month between summer and winter monsoons, considering vestiges of low SLP in the southwestern Bay of Bengal and the related cyclonic circulation. A hypothesis for the origin—or the lingering—of low SLP in the bay in October is currently being evaluated from observational analysis.

[2] Early retreat of the westerlies over the South China Sea relative to the Bay of Bengal was reported by Matsumoto (1997) as well, although at pentad resolution.

[3] Of the four, the APHRODITE v1101 data are the most restrictive because they end in December 2007.
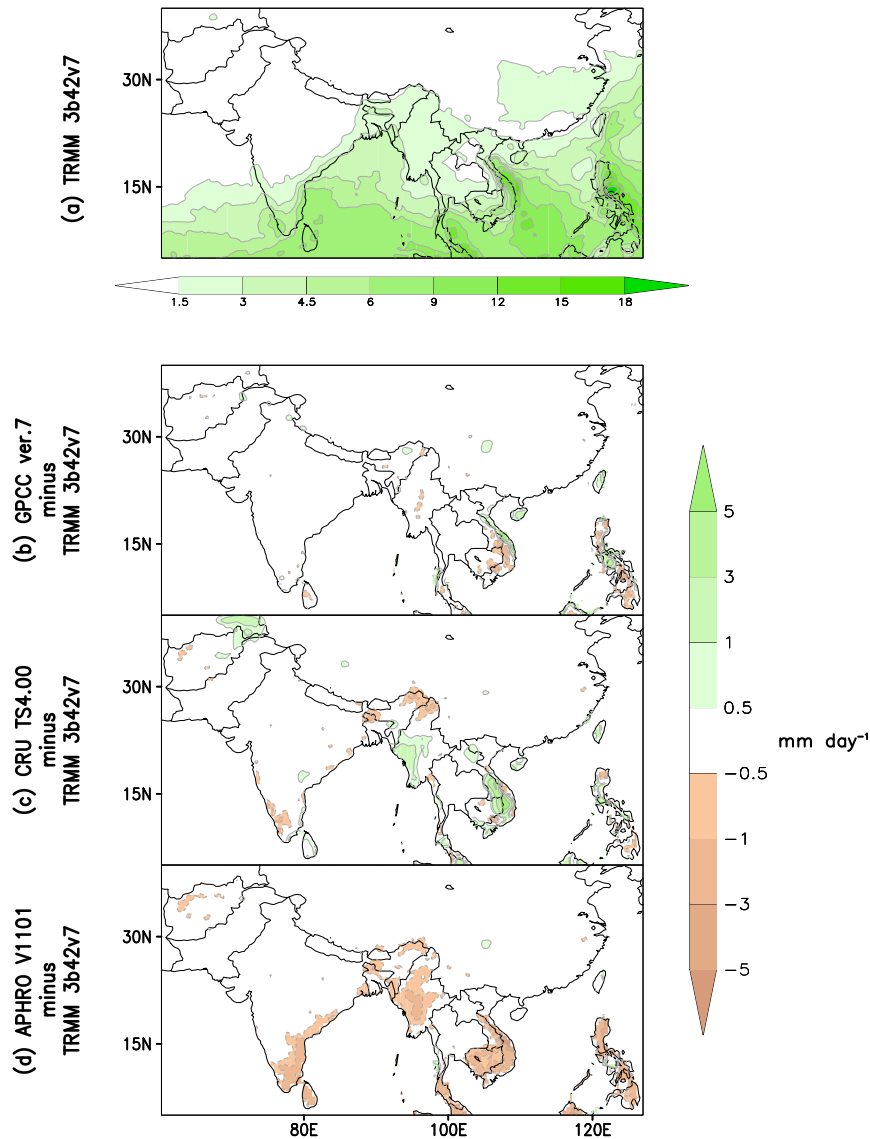
FIG. 4. Climatological OND seasonal rainfall (1998–2007) (a) from TRMM, 3B42v7, and the difference (b) between GPCC, version 7, and TRMM, (c) between CRU-TS4.00 and TRMM, and (d) between APHRODITEv1101 and TRMM. For (a), the CI is 1.5 mm day^{-1} for values < 6.0 mm day^{-1} and 3.0 mm day^{-1} for higher values. For (b), (c), and (d), the CI is 0.5 mm day^{-1} for values < 1.0 mm day^{-1} and 2.0 mm day^{-1} for higher values. The shading threshold is 1.5 mm day^{-1} for (a) and 0.5 mm day^{-1} for (b), (c), and (d). The fields are displayed after one application of smth9 in GrADS.

OND months span the NEM season, regions other than the NEM regions also have rainfall in this period, just not their peak rainfall. The NEM regions noted earlier (the red arrow regions in Fig. 1b) are apparent in Fig. 4a when attention is restricted to the regions where OND rainfall is larger than 4.5 mm day^{-1} (the third contour). Of the three in situ datasets, GPCC (Fig. 4b) is in closest agreement with TRMM but for the differences over Vietnam where in situ data are unable to resolve the

influence of narrow coastal orography on regional rainfall—more rain on the windward side (i.e., to the east, in view of the prevailing northeasterlies) with a rain shadow to the west. The CRU rainfall (Fig. 4c) is positively biased with respect to TRMM, especially over Myanmar, Laos, Cambodia, and Vietnam where the bias is in the 0.5–3 mm day^{-1} range. The APHRODITE rainfall (Fig. 4d), on the other hand, exhibits a dry bias of similar range with respect to TRMM, notably over the

core NEM regions (peninsular India, Sri Lanka, Southeast Asia, and the Philippines). The intercomparison indicates some preference for the GPCC precipitation analysis in documentation of the longer-period NEM climatology and interannual variability.

4. The NEM in historical climate simulations

a. Simulation of seasonal cycle

The simulations of twentieth-century (i.e., historical) climate provide a unique opportunity for the evaluation of models whose projections of future climate form the backbone of the IPCC-AR5 (Flato et al. 2013). The annual mean and annual cycle of rainfall, obtained from harmonic analysis of the climatological monthly rainfall in five historical simulations, is shown in Fig. 5; the TRMM precipitation analysis (Fig. 1b; and reproduced in Fig. 5a to facilitate comparison) is the target for these simulations. Although the simulated hydroclimate can be comprehensively critiqued using harmonic plots—for example, both summer and winter monsoons can be assessed—the focus here is on the NEM, whose amplitude and temporal phase is visually highlighted using red arrows in Fig. 5 (as in Fig. 1b).

The NCAR-CCSM4 simulation (Fig. 5b) of the winter monsoon is reasonable but for the lack of confinement of the monsoon region to near-coastal waters; for example, the NEM region is unrealistically expansive over the South China Sea and even over the north-equatorial Indian Ocean. The temporal phasing is also a bit off in view of the lack of southeastward orientation of the arrows off the tip of the Indian Peninsula. The NCAR simulation is not without other deficiencies—notably, the absence of intense summer monsoon precipitation along the southwest coast of India and the west coast of Myanmar and Thailand, which is likely from the lack of model resolution of the narrow orographic features in these regions (e.g., the Western Ghats). Likely related to this deficiency is the overrepresentation of summer monsoon precipitation over the Himalayan region and the northern Indo-Gangetic Plain. The GFDL CM3 simulation (Fig. 5c) of the NEM is like NCAR's but more deficient along the Vietnam coast where the peak rainfall month in the simulation is in late summer rather than in midautumn. The distribution of the rainfall annual mean in the GFDL simulation, again, shows the impact of unresolved orography, even the Himalayan–Tibetan complex, to an extent.

The UKMO HadCM3 simulation departs the most from the observed rainfall distribution (Fig. 5d). Although it has some vestiges of the NEM, the annual-mean rainfall is underestimated in the west (Indian subcontinent) and overestimated in the east (South China Sea); the lack of intense precipitation zones over the continent, likely, results from the coarse model resolution (see Table 1). The other UKMO model (HadGEM2-ES; Fig. 5e) underestimates even more the rainfall annual mean over western and peninsular India. Despite this dry bias (reflected also in the reduced red-arrow amplitudes along the southeastern coast), the NEM timing and its eastward extent over the Bay of Bengal and the South China Sea are well represented. The model's finer resolution allows a quasi-realistic representation of the intense precipitation along Myanmar's coast and over the northeastern Indian subcontinent. The MPI-ESM-LR simulation (Fig. 5f) captures aspects of the NEM and the larger rainfall distribution. Notable departures include an expansive NEM over the South China Sea and the shifted location of rainfall maxima, for example, a northward shift over the northeastern Indian subcontinent and a southward one along the Myanmar coast.

b. Simulation of OND rainfall

The models' skill in simulating the October–December rainfall over South and Southeast Asia and the adjacent seas/bays is assessed in Fig. 6, which compares the OND period climatology in the common period of the historical simulations and TRMM dataset (1998–2005). The model rainfall climatology is shown as the difference from the TRMM one (Fig. 4a; the validation target). Focusing on the NEM regions, the bias in simulations is large and extensively distributed over peninsular India and Vietnam and the southwestern Bay of Bengal and the South China Sea. Over peninsular India, the bias is generally negative, especially in the Hadley simulations, which underestimate rainfall by as much as 50%; the NCAR simulation is the only one overestimating NEM rainfall. All five simulations underestimate the OND rainfall over Vietnam and its coastal zone and overestimate rainfall over the central-eastern South China Sea. The OND rainfall bias over Sri Lanka is similar to that over peninsular India: positive in the NCAR simulation and negative in the others, with GFDL being neutral in this regard.

5. Influence of ENSO on the NEM rainfall

The influence of ENSO on the South Asian summer monsoon—the southwest monsoon—has been extensively documented since the pioneering analysis of Rasmusson and Carpenter (1983) and Sikka (1980) and used in the dynamical and statistical predictions of summer monsoon rainfall over the Indian subcontinent. The summer preceding the peak warm phase of ENSO—El Niño—shows impressive rainfall deficits over the entire
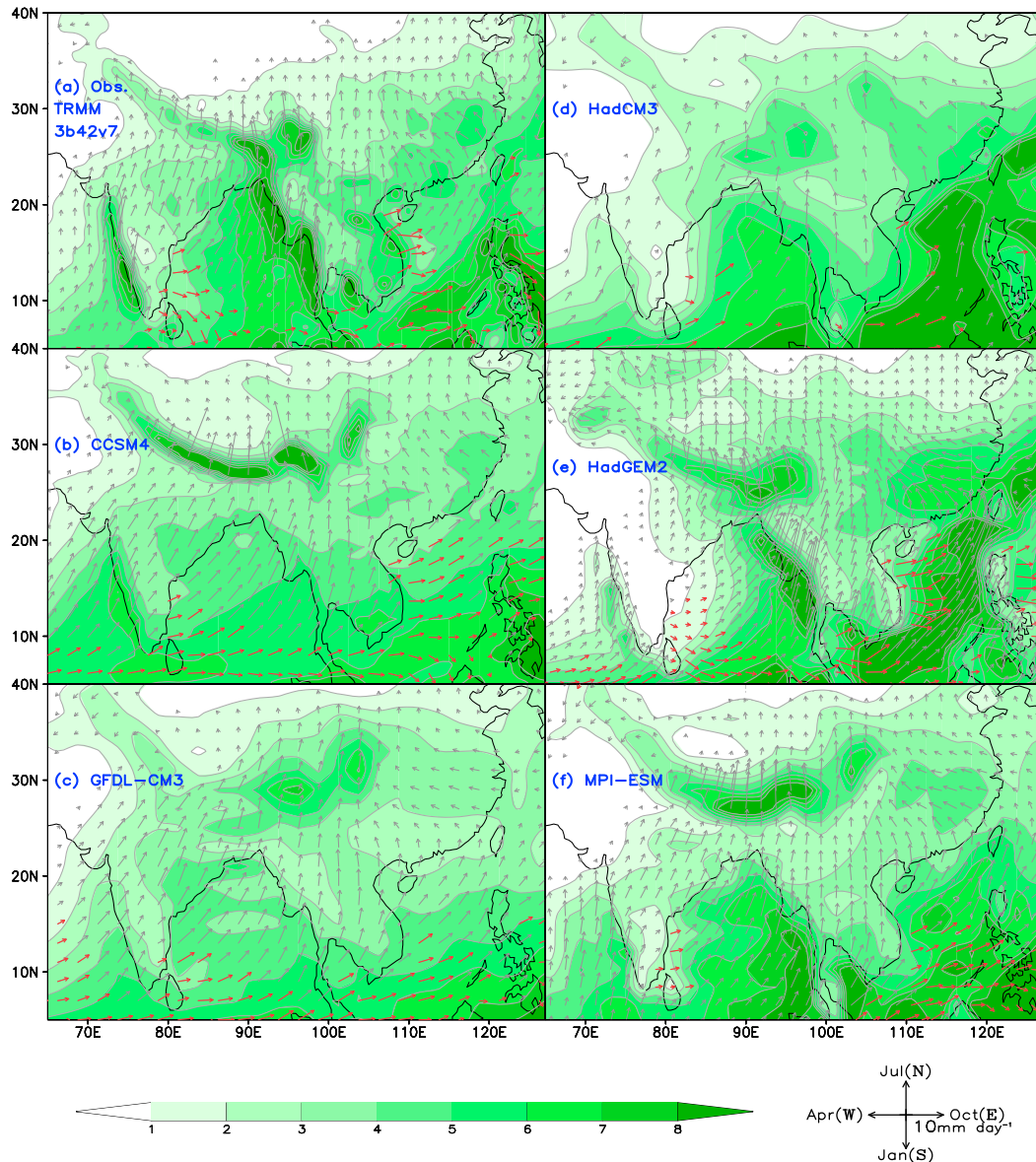
FIG. 5. Climatological rainfall in five IPCC-AR5 historical climate model simulations (1986–2005). (a) The climatological precipitation from TRMM, 3B42v7 (1998–2016)—the observational target. (b)–(f) The average field across all ensemble members of each simulation. Vectors represent annual cycle (first harmonic), and contours show annual mean (mm day^{-1}). Vector scaling and the phase of the annual cycle are shown at the bottom right; vectors pointing north indicate July as the maximum rainfall month, and so on. Vectors in red represent regions receiving winter monsoon (OND) rainfall. The rainfall annual mean is contoured and shaded at 1.0 mm day^{-1} intervals. The amplitude threshold for plotting vectors is 0.75 mm day^{-1}. Because the observational dataset is on a much finer resolution than are the model fields, (a) is shown after four applications of smth9 in GrADS.

subcontinent; the following summer also exhibits deficits but only over the eastern–northeastern subcontinent.

El Niño's influence on the northeast winter monsoon has also been investigated from observational analysis: The NEM was shown to strengthen during the ENSO build-up year, that is, above-normal autumn precipitation over southeastern peninsular India and Sri Lanka (Rasmusson and Carpenter 1983; Ropelewski and Halpert 1987). A closer examination of how Sri Lanka's rainfall distribution is impacted was undertaken by Suppiah (1997). The present analysis expands on these studies, principally, in three ways. First, it shows the ENSO impact on the larger NEM region, one that includes eastern Indochina and the Philippines, in
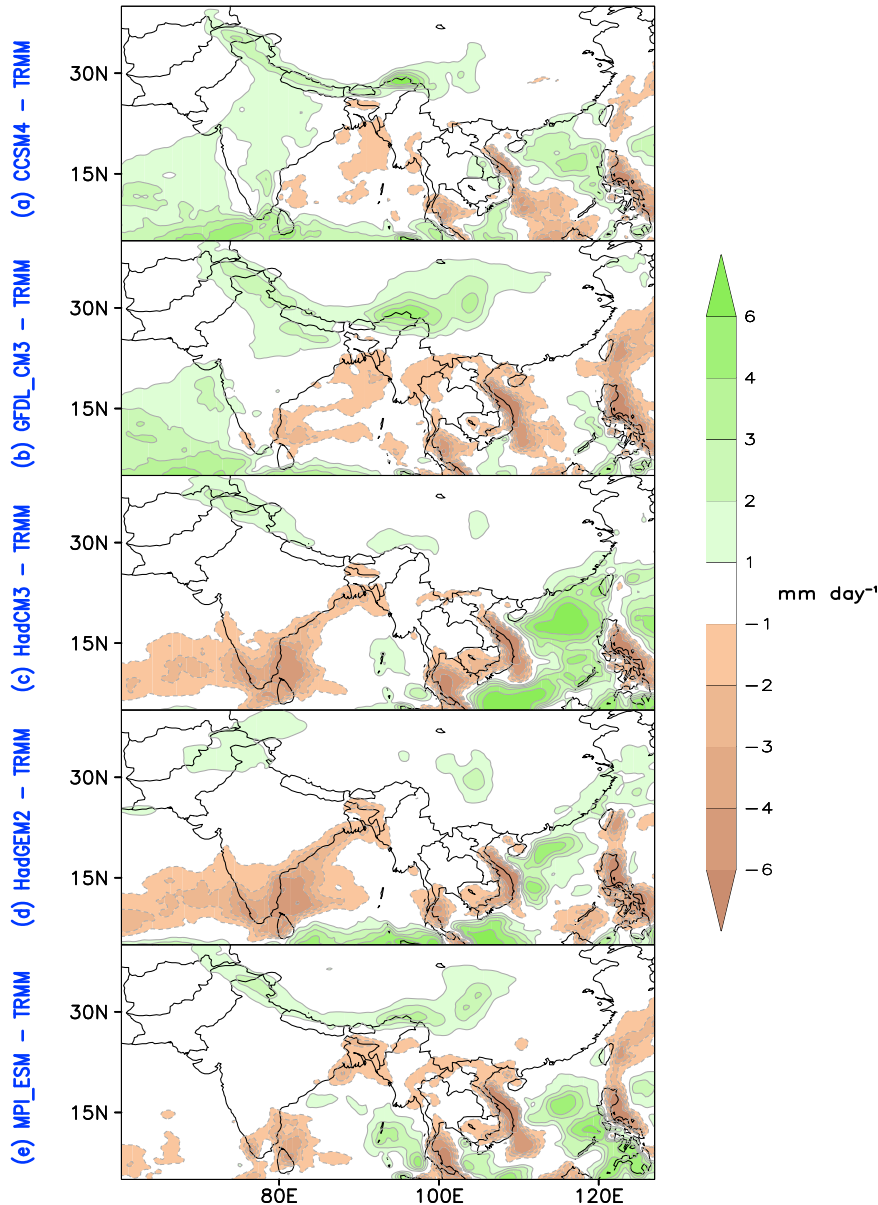
FIG. 6. Climatological OND seasonal rainfall (1998–2005) in five IPCC-AR5 historical cli-
mate model simulations evaluated against TRMM, 3B42v7, observations: (a) NCAR CCSM4,
(b) NOAA GFDL CM3, (c) UKMO HadCM3, (d) UKMO HadGEM2-ES, and (e) MPI-ESM-
LR. The CI and shading threshold is 1.0 mm day^{-1}. The fields are displayed after two appli-
cations of smth9 in GrADS.

addition to peninsular India and Sri Lanka. Second, instead
of compositing, it uses objective analysis based on linear
regressions on the Niño-3.4 SST index to extract the ENSO
influence. Last, it documents, perhaps, for the first time, the
subseasonal variation of the ENSO influence, all in Fig. 7.

a. The ENSO influence in observations

The influence of El Niño on the NEM is obtained from
rainfall regressions on the winter Niño-3.4 SST index, as

discussed in section 2e. The influence on OND rainfall
(Fig. 7a) is essentially confined to the core NEM re-
gions: southeastern peninsular India and Sri Lanka with
above-normal rainfall and, farther to the east, eastern
Indochina and the Philippines with below-normal rain-
fall. The ENSO influence is significant: Over India and
Sri Lanka, the regressions are ~0.4 mm day^{-1} per unit
index, which translates into a rainfall anomaly of
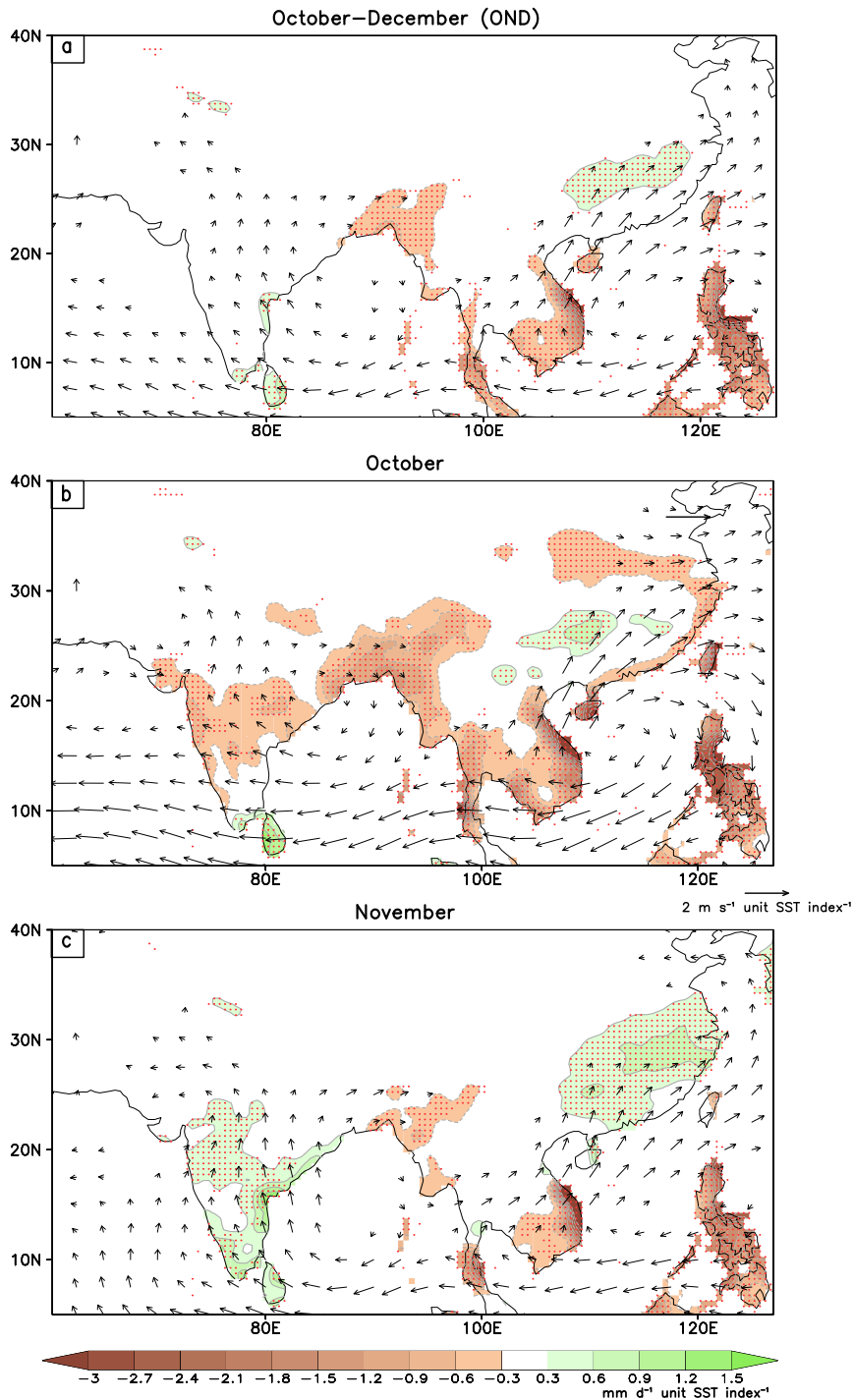~0.8 mm day^{-1} for a strong El Niño episode (Niño-3.4

FIG. 7. Characteristic influence of ENSO on winter monsoon rainfall and 925-hPa winds from observations for (a) the OND season and the months of (b) October and (c) November. The influence is obtained from temporally leading regressions of rainfall (GPCC, version 7) and winds (NCEP reanalysis) on the winter (DJF averaged) Niño-3.4 SST anomaly index (constructed from HadISST1.1) in the post-IGY period (1958–2013). Green contours represent rainfall surplus, and brown contours represent deficit. The CI is $0.3\,\mathrm{mm\,day^{-1}}$ per unit of normalized SST index. Regressions are shown after one application of smth9 in GrADS. Regressions that are significant at the 95% level are stippled.

SST index of $\sim$2). Comparison with the regional OND climatology ($\sim$5 mm day^{-1}; cf. Fig. 4a) indicates that the anomalies are significant, being $\sim$16% of the climatology. Likewise, anomalies over eastern Vietnam are $\sim$1.5 mm day^{-1} per unit index, or $\sim$3 mm day^{-1} for a strong episode, while the regional OND climatology is 12–15 mm day^{-1} (cf. Fig. 4a). Outside the core monsoon region, the ENSO influence on the seasonally averaged (OND) rainfall is modest.

The ENSO influence on the NEM low-level (925 hPa) circulation is also shown in Fig. 7. The seasonal (OND; Fig. 7a) influence consists of weak anticyclonic flows: one centered over the Bay of Bengal with easterlies ($\sim$0.8 m s^{-1} per unit SST index) in the deep tropics and weak southeasterlies over peninsular India and another over the South China Sea associated with southwesterly flow over Southeast Asia and eastern China ($\sim$1 m s^{-1} per unit SST index).

The subseasonal variation in ENSO's influence is documented from separate regressions of the October and November rainfall (Figs. 7b,c). The October influence (Fig. 7b), especially the rainfall deficit over the western-central and northeastern subcontinent, is broadly similar to El Niño–related anomalies in summer monsoon rainfall in the ENSO development year (Rasmusson and Carpenter 1983), generating an impression that the summer monsoon season (June–September in climatological rainfall) continues for an additional month, at least, in the context of the ENSO influence. In the NEM regions, El Niño generates positive anomalies in October rainfall over southeastern peninsular India and Sri Lanka, and negative ones over Indochina and the Philippines. The ENSO wind regressions consist of robust anticyclonic flow over the South China Sea, with easterlies ($\sim$0.8–1.2 m s^{-1} per unit index) over lower Indochina and southwesterlies to the north; wind regressions over peninsular India are also strong and primarily easterly.

El Niño's influence on November rainfall (Fig. 7c) shows positive anomalies over peninsular India, especially in its southeastern sector (Kerala, Tamil Nadu, and Andhra Pradesh, India), and negative ones over southeastern Indochina and the Philippines, the latter much as in October. Farther to the north over peninsular India, the November anomalies (positive) are quite opposite of the October ones—an impressive subseasonal variation in ENSO's rainfall influence that is concealed in the OND average. The November anomalies are significant and positive also over eastern China, and the ones over Bangladesh and Myanmar, while negative, are relatively positive vis-à-vis the October ones. ENSO's November wind regressions depict a well-developed anticyclonic flow structure over the Bay of Bengal, with southerly flow over peninsular India—in

contrast with the ENSO-related easterly anomalies in the preceding month.

b. The ENSO influence mechanism

The mechanisms by which El Niño SST anomalies in the central-eastern equatorial Pacific influence the northeast winter monsoon rainfall are briefly investigated in this section. The vertically averaged (1000–100 hPa) diabatic heating Q_D, residually diagnosed from ERA-Interim, and the lower-tropospheric streamfunction ψ_{850} anomalies are examined in November when El Niño's influence on peninsular India is strongest (cf. Fig. 7). As before, the anomalies are obtained from the temporally leading regressions on the DJF Niño-3.4 SST index.

The ENSO-related November diabatic heating anomalies (Fig. 8) are positive in the central-eastern equatorial Pacific (approaching +1.0 K day^{-1} per unit SST index) and negative over the Maritime Continent, northwestern tropical Pacific (including Indochina and the Philippines), and the South Pacific convergence zone, in line with their earlier characterization (Nigam et al. 2000). Superposed ψ_{850} contours in Fig. 8 characterize the low-level rotational circulation response, which consists of cyclonic circulation straddling the equator in the central basin, leading to equatorial westerlies in the heating anomaly longitudes. Likewise, a pair of anticyclones straddle the equator in the eastern Indian Ocean basin, with related easterlies. The rotational response has some resemblance with the response of deep convective heating in the Matsuno–Gill model (Matsuno 1966; Gill 1980). This model is, however, unable to realistically model the divergent response, as noted in Nigam and Shen (1993),[4] and, of course, the near-surface wind response under the large-scale subsidence zones over tropical basins (Lindzen and Nigam 1987).

The characterization of El Niño–related low-level winds in the global tropics (Fig. 8) facilitates understanding of how El Niño's influence on NEM rainfall is generated: The anticyclonic circulation over the Indian Ocean (notably in Fig. 7c)—key to onshore moisture transports over peninsular India and the resulting orography-mediated positive rainfall anomalies in the core NEM regions—is itself a key element of El Niño's widely modeled tropical atmospheric response (Watanabe and Jin 2002, their Fig. 2a; Wang and Zhang 2002, their Figs. 6c,d) to reduced convection over the Maritime

---

[4] The low-level convergence over the heating maximum is generated mostly from meridional convergence (i.e., $\partial v/\partial y$) in nature but not in the Matsuno–Gill model where zonal convergence (i.e., $\partial u/\partial x$) remains dominant.
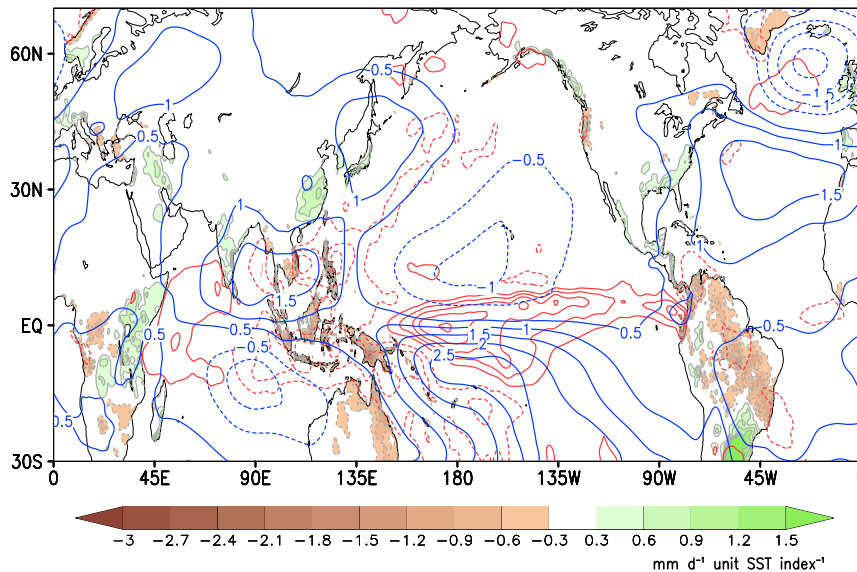
FIG. 8. Changes in precipitation, vertically averaged (1000–100 hPa) diabatic heating, and 850-hPa streamfunction for November associated with ENSO. The response is obtained from temporally leading regressions of precipitation (GPCC, version 7), vertically averaged diabatic heating, and streamfunction (both fields diagnosed from ERA-Interim) on the winter (DJF averaged) Niño-3.4 SST anomaly index for November (1980–2013). Green contours represent rainfall surplus, and brown contours indicate deficit; The CI is 0.3 mm day^{-1} per unit SST index. Solid red contours represent positive diabatic heating anomalies, and dashed red contours represent negative diabatic heating anomalies; The CI is 0.2 K day^{-1} per unit SST index. Solid blue contours represent positive 850-hPa streamfunction anomalies, and dashed blue contours are for negative 850-hPa streamfunction anomalies; The CI is 0.5×10^6 m^2 s^{-1} per unit SST index.

Continent and adjoining regions (northwestern tropical Pacific and Southeast Asia).

c. ENSO influence on the NEM rainfall record

The rainfall anomalies over southeastern peninsular India and Sri Lanka—a core NEM region marked in red in Fig. 3, top panel—is plotted in Fig. 9 both for October and November and for the OND period. Also plotted is the winter (December–February) Niño-3.4 SST index in red. The index exceeds +2.0 during 1982–83 and 1997–98, marking major episodes of the recent period; the most recent one, in 2015–16, when the index was even higher (~+3.0) is not shown because the GPCC rainfall record ends in December 2013. The ENSO index is correlated with October rainfall at +0.11 and with the November and OND rainfall at +0.29 and +0.29, respectively; the latter two are statistically significant at the 95% level. The low October correlation is not unexpected, given the very limited footprint of the ENSO precipitation anomalies in the core NEM region (Fig. 7b).

d. The ENSO influence on NEM rainfall in historical simulations

The rendition of ENSO's influence on the NEM rainfall in the IPCC-AR5 historical simulations is

documented in Fig. 10, notwithstanding the significant biases in the modeled NEM rainfall climatologies (cf. Fig. 6). Rainfall regressions on the Niño-3.4 SST index (obtained from the related SST simulation) were computed for each ensemble member and then averaged across all simulations of each model. The El Niño influence on NEM rainfall is evidently very weak in the simulations, especially over continents where the impact is below the contouring threshold (0.3 mm day^{-1} per unit index); lowering the threshold by one-half was also unproductive. Two of the five simulations [NCAR (Fig. 10a) and MPI (Fig. 10e)] do contain a weak signal over southeastern peninsular India but of the wrong sign. El Niño's influence over eastern Indochina is, however, correctly represented signwise, but again with weaker amplitude. Unfortunately, the TRMM rainfall record is too short for the extraction of the characteristic El Niño influence on oceanic precipitation. In the absence of a validation target, the veracity of the simulated El Niño–related rainfall deficit over the South China Sea remains unassessed.

6. Trends in NEM rainfall

Historical precipitation trends over Southeast Asia have been investigated from an extensive suite of
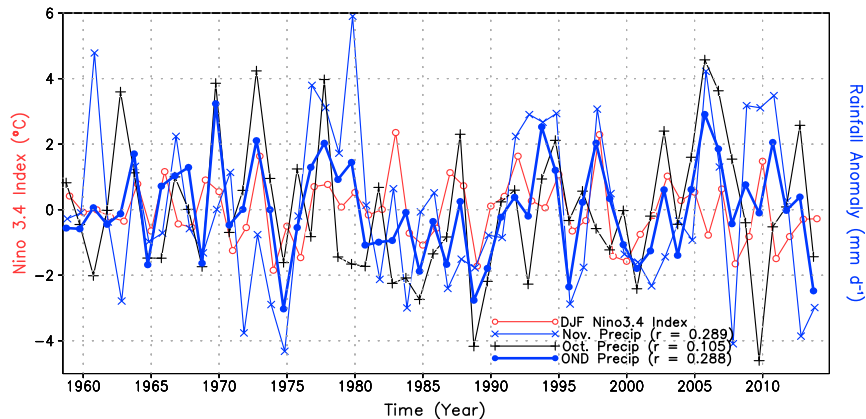
FIG. 9. Correlation between Niño-3.4 SST index and NEM rainfall anomaly time series over southeastern peninsular India and Sri Lanka. The Niño-3.4 SST index (°C) is obtained from HadISST1.1, and GPCC, version 7, provides the observed rainfall anomaly (mm day^{-1}). The period of analysis is 1958–2013. November rainfall anomaly is shown using the solid blue line with times signs, October uses the solid black line with plus signs, and OND uses the thick blue line with closed circles. The rainfall anomaly in each case is the area-averaged value computed from continental grid points with SD exceeding 1.5 mm day^{-1}. The correlation between the rainfall and Niño-3.4 SST time series is noted within parentheses.

meteorological stations in previous studies. Heavy precipitation was shown to increase (decrease) in southern (northern) Vietnam (Endo et al. 2009). Trends in extreme precipitation in the Philippines were assessed by Villafuerte et al. (2014). The present study is focused on the seasonal winter monsoon (OND) precipitation trends and thus is not limited to extreme events. The NEM rainfall is analyzed in the post-IGY period (1958–2013) to uncover potential trends in this 56-yr record over the NEM regions (eastern Indochina, the Philippines, peninsular India, and Sri Lanka); the OND trends are displayed in Fig. 11.

In focusing on the core NEM regions, positive trends are found over southern Vietnam, the Philippines, Malaysia, and southern and eastern peninsular India. The trends are larger than 1.5 mm day^{-1} (100 yr)$^{-1}$ and statistically significant (at the 95% level) over southern Vietnam, reflecting an ~0.84 mm day^{-1} increase in OND rainfall in the post-IGY period. The increase is notable as climatological rainfall in these months is ~4.5–6.0 mm day^{-1}; the IGY-period trends thus represent, approximately, a 15%–20% increase in OND rainfall in this region. Over the southeastern Philippines, significant positive trend larger than 2.0 mm day^{-1} (100 yr)$^{-1}$ reflects a 15% increase in OND rainfall. Meanwhile, over peninsular India, the NEM trends are not statistically significant; however, trends are not declining, being typically larger than +1.0 mm day^{-1} (100 yr)$^{-1}$. Notable trends in OND rainfall are also present outside the NEM regions, but these are not as consequential because OND is not the peak rainfall

season there, for example, the drying trend in the Irrawaddy River basin (Myanmar).

The origin of the modest post-IGY increase in NEM rainfall over coastal Vietnam was briefly investigated from analysis of the near-surface (925 hPa) wind trend, drawing on the basic notion of the monsoon as being driven by onshore moisture-laden winds. Although uncertainties in the early-period upper-air winds, especially over the oceans, preclude attribution, in some regions, such as eastern Indochina, a positive northeasterly wind trend is evident. No such trend is, however, present over peninsular India, another region of positive rainfall trends.

7. Concluding remarks

The northeast winter monsoon, the diminutive cousin of the southwest summer monsoon, brings seasonal (winter) rains to the eastern coast of peninsular India, Indochina, and the Philippines. The low-level northeasterly winds impinge on the eastern coasts after gathering moisture over the upstream bays and seas, for example, the Bay of Bengal in the case of peninsular India, and the South China Sea in the case of eastern Indochina. The onshore moisture influx is a necessary but not sufficient condition; flux convergence is needed for rainfall, with orographic interaction often generating the convergent conditions, for example, with the Eastern Ghats over peninsular India. Quite like the teeming Indo-Gangetic Plain where the southwest monsoon brings bountiful rain in summer, the populous eastern
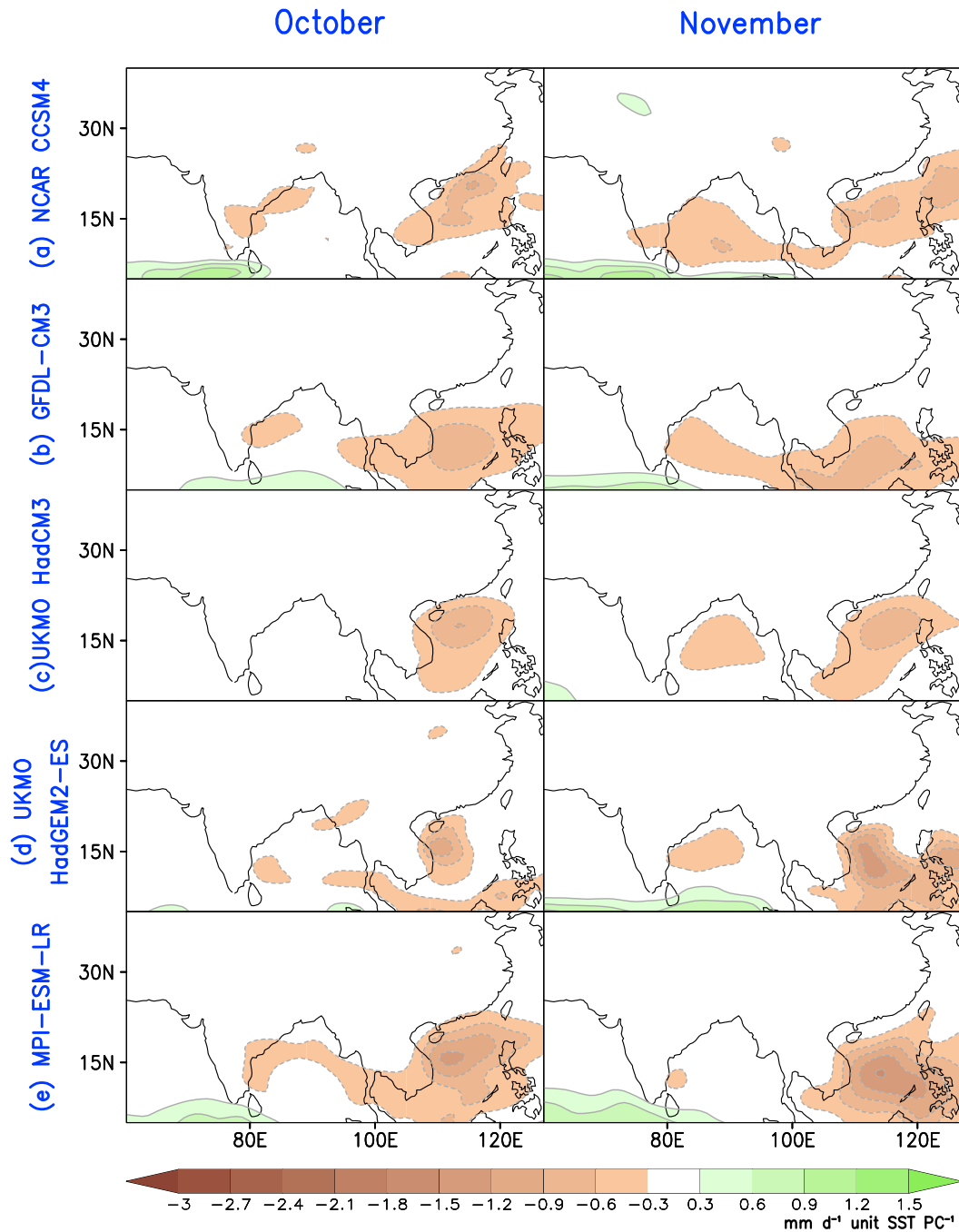
FIG. 10. Characteristic influence of ENSO on winter monsoon rainfall in five IPCC-AR5 historical climate model simulations for the months of October and November; the influence is obtained from temporally leading regressions of precipitation on the winter Niño-3.4 SST anomaly index (constructed from model SST simulations) in the post-IGY period (1958–2004). (a)–(e) The average field across all ensemble members of each simulation. Green contours represent rainfall surplus, and brown contours indicate deficit. The CI is 0.3 mm day^{-1} per (unit SST index). Regressions are shown after one application of smth9 in GrADS.

coastal regions depend on the NEM for life and sustenance. The NEM has, however, received less research attention, motivating this observational analysis that focuses on the NEM's climatological evolution at monthly resolution, its interannual variability, and long-term trend.

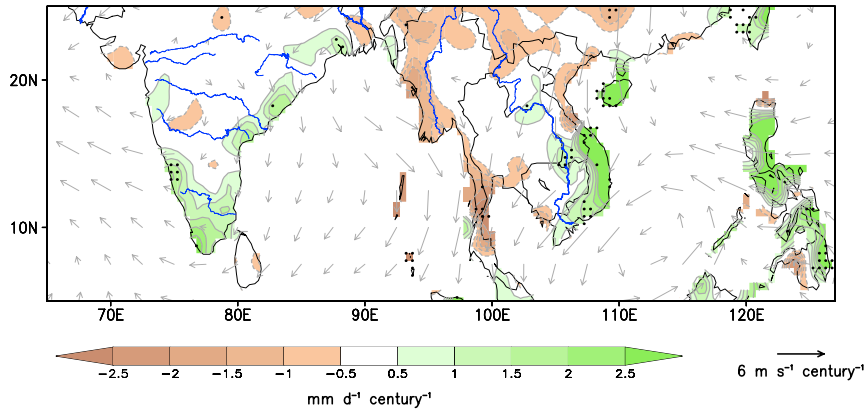Given the complex orography and narrow coastal zones in the NEM domain, the longer period in situ

FIG. 11. Linear trend in winter monsoon (OND) rainfall and 925-hPa winds (1958–2013). Rainfall trend is based on GPCC, version 7, and winds are from the NCEP reanalysis. Green contours represent positive rainfall trend values, and brown contours are for negative rainfall trend values. The CI and shading threshold is $0.5 \, \text{mm day}^{-1} \, (100 \, \text{yr})^{-1}$. Rainfall trend is shown after one application of smth9 in GrADS. Trends significant at the 95% level are stippled in black.

precipitation analyses were first assessed from intercomparison with the recent period Tropical Rainfall Measuring Mission's (TRMM) precipitation. The overlap period comparisons showed the Global Precipitation Climatology Center's (GPCC) in situ analysis to have the least bias, prompting its further use in the interannual variability and trend analysis; the CRU-TS4.00 slightly overestimates precipitation over southern Myanmar and Indochina, and the APHRODITE v1101 analysis exhibits a dry bias over the core NEM regions.

Below are the four major findings of this study.

1) We demarcated the NEM core regions from harmonic analysis of climatological monthly precipitation data, both in situ (GPCC) and remotely sensed (TRMM).

2) We documented the monthly evolution of the NEM from analysis of rainfall, sea level pressure, and low-level winds. A key finding here is the asynchronicity in the establishment of northeasterlies over the Bay of Bengal and the South China Sea; the northeasterlies appear over the Bay of Bengal in November, that is, a month later than over the South China Sea.

3) We showed El Niño–Southern Oscillation's impact on NEM rainfall to be significant: The El Niño phase leads to a stronger NEM rainfall over southeastern peninsular India and Sri Lanka but diminished rainfall over Thailand, Vietnam, and the Philippines. An interesting finding here is that the impact varies subseasonally, being weak in October and strong in November. The positive rainfall anomalies over peninsular India are generated by the anticyclonic flow centered over the Bay of Bengal, which is forced by El Niño–related reduction in deep convection over the Maritime Continent.

4) We found that the historical twentieth-century climate simulations informing the IPCC-AR5 show varied deficiencies in the NEM rainfall distribution and a markedly weaker (and often unrealistic) ENSO–NEM rainfall relationship.

Statistical and dynamical predictions of the NEM rainfall over peninsular India and Sri Lanka are in relative infancy vis-à-vis the southwest summer monsoon. Perhaps this analysis of El Niño–Southern Oscillation impacts, and especially their subseasonal variation, will reinvigorate these efforts, bringing hydroclimate relief to millions.

REFERENCES

Akasaka, I., 2010: Interannual variations in seasonal march of rainfall in the Philippines. *Int. J. Climatol.*, **30**, 1301–1314, https://doi.org/10.1002/joc.1975; Corrigendum, **31**, 1413, https://doi.org/10.1002/joc.2377.

——, W. Morishima, and T. Mikami, 2007: Seasonal march and its spatial difference of rainfall in the Philippines. *Int. J. Climatol.*, **27**, 715–725, https://doi.org/10.1002/joc.1428.

Becker, A., P. Finger, A. Meyer-Christoffer, B. Rudolf, K. Schamm, U. Schneider, and M. Ziese, 2013: A description of the global land-surface precipitation data products of the Global Precipitation Climatology Centre with sample applications including centennial (trend) analysis from 1901–present. *Earth Syst. Sci. Data*, **5**, 71–99, https://doi.org/10.5194/essd-5-71-2013.

Bjerknes, J., 1969: Atmospheric teleconnections from the equatorial Pacific. *Mon. Wea. Rev.*, **97**, 163–172, https://doi.org/10.1175/1520-0493(1969)097<0163:ATFTEP>2.3.CO;2.

Bollasina, M., and S. Nigam, 2009: Indian Ocean SST, evaporation, and precipitation during the South Asian summer monsoon in IPCC-AR4 coupled simulations. *Climate Dyn.*, **33**, 1017–1032, https://doi.org/10.1007/s00382-008-0477-4.

Chan, S. C., and S. Nigam, 2009: Residual diagnosis of diabatic heating from ERA-40 and NCEP reanalyses: Intercomparisons with TRMM. *J. Climate*, **22**, 414–428, https://doi.org/10.1175/2008JCLI2417.1.

Chen, T.-C., J.-D. Tsay, M.-C. Yen, and J. Matsumoto, 2012: Interannual variation of the late fall rainfall in central Vietnam. *J. Climate*, **25**, 392–413, https://doi.org/10.1175/JCLI-D-11-00068.1.

De, U. S., and R. K. Mukhopadhyay, 1999: The effect of ENSO/anti-ENSO on northeast monsoon rainfall. *Mausam*, **50**, 343–354.

Dee, D. P., and Coauthors, 2011: The ERA-Interim reanalysis: Configuration and performance of the data assimilation system. *Quart. J. Roy. Meteor. Soc.*, **137**, 553–597, https://doi.org/10.1002/qj.828.

Dhar, O. N., and P. R. Rakhecha, 1983: Foreshadowing northeast monsoon rainfall over Tamil Nadu, India. *Mon. Wea. Rev.*, **111**, 109–112, https://doi.org/10.1175/1520-0493(1983)111<0109:FNMROT>2.0.CO;2.

Endo, H., and A. Kitoh, 2016: Projecting changes of the Asian summer monsoon through the twenty-first century. *The Monsoons and Climate Change: Observations and Modeling*, L. M. V. Carvalho and C. Jones, Eds., Springer, 47–66.

Endo, N., J. Matsumoto, and T. Lwin, 2009: Trends in precipitation extremes over Southeast Asia. *SOLA*, **5**, 168–171, https://doi.org/10.2151/sola.2009-043.

Flato, G., and Coauthors, 2013: Evaluation of climate models. *Climate Change 2013: The Physical Science Basis*, T. F. Stocker et al., Eds., Cambridge University Press, 741–866, http://www.ipcc.ch/pdf/assessment-report/ar5/wg1/WG1AR5_Chapter09_FINAL.pdf.

Gill, A. E., 1980: Some simple solutions for heat-induced tropical circulation. *Quart. J. Roy. Meteor. Soc.*, **106**, 447–462, https://doi.org/10.1002/qj.49710644905.

Harris, I., P. D. Jones, T. J. Osborn, and D. H. Lister, 2014: Updated high-resolution grids of monthly climatic observations—The CRU TS3.10 dataset. *Int. J. Climatol.*, **34**, 623–642, https://doi.org/10.1002/joc.3711.

He, S., and H. Wang, 2013: Oscillating relationship between the East Asian winter monsoon and ENSO. *J. Climate*, **26**, 9819–9838, https://doi.org/10.1175/JCLI-D-13-00174.1.

Huffman, G. J., and Coauthors, 2007: The TRMM multisatellite precipitation analysis (TMPA): Quasi-global, multiyear, combined-sensor precipitation estimates at fine scales. *J. Hydrometeor.*, **8**, 38–55, https://doi.org/10.1175/JHM560.1.

——, R. F. Adler, D. T. Bolvin, and E. J. Nelkin, 2010: The TRMM Multi-satellite Precipitation Analysis (TMPA). *Satellite Rainfall Applications for Surface Hydrology*, F. Hossain and M. Gebremichael, Eds., Springer Verlag, 3–22.

Jayanthi, N., and S. Govindachari, 1999: El Niño and NE monsoon rainfall over Tamilnadu. *Mausam*, **50**, 217–218.

Kalnay, E., and Coauthors, 1996: The NCEP/NCAR 40-Year Reanalysis Project. *Bull. Amer. Meteor. Soc.*, **77**, 437–471, https://doi.org/10.1175/1520-0477(1996)077<0437:TNYRP>2.0.CO;2.

Kumar, P., K. R. Kumar, M. Rajeevan, and A. K. Sahai, 2007: On the recent strengthening of the relationship between ENSO and northeast monsoon rainfall over South Asia. *Climate Dyn.*, **28**, 649–660, https://doi.org/10.1007/s00382-006-0210-0.

Lindzen, R. S., and S. Nigam, 1987: On the role of sea surface temperature gradients in forcing low-level winds and convergence in the tropics. *J. Atmos. Sci.*, **44**, 2418–2436, https://doi.org/10.1175/1520-0469(1987)044<2418:OTROSS>2.0.CO;2.

Matsumoto, J., 1990: The seasonal changes of wind fields in the global tropics. *Geogr. Rev. Japan*, **63B**, 156–178, https://doi.org/10.4157/grj1984b.63.156.

——, 1997: Seasonal transition of summer rainy season over Indochina and adjacent monsoon region. *Adv. Atmos. Sci.*, **14**, 231–245, https://doi.org/10.1007/s00376-997-0022-0.

Matsuno, T., 1966: Quasi-geostrophic motions in the equatorial area. *J. Meteor. Soc. Japan*, **44**, 25–43, https://doi.org/10.2151/jmsj1965.44.1_25.

Menon, A., A. Levermann, J. Schewe, J. Lehmann, and K. Frieler, 2013: Consistent increase in Indian monsoon rainfall and its variability across CMIP-5 models. *Earth Syst. Dyn.*, **4**, 287–300, https://doi.org/10.5194/esd-4-287-2013.

Nigam, S., and H.-S. Shen, 1993: Structure of oceanic and atmospheric low-frequency variability over the tropical Pacific and Indian Oceans. Part I: COADS observations. *J. Climate*, **6**, 657–676, https://doi.org/10.1175/1520-0442(1993)006<0657:SOOAAL>2.0.CO;2.

——, and A. Ruiz-Barradas, 2006: Seasonal hydroclimate variability over North America in global and regional reanalyses and AMIP simulations: Varied representation. *J. Climate*, **19**, 815–837, https://doi.org/10.1175/JCLI3635.1.

——, C. Chung, and E. DeWeaver, 2000: ENSO diabatic heating in ECMWF and NCEP–NCAR reanalyses, and NCAR CCM3 simulation. *J. Climate*, **13**, 3152–3171, https://doi.org/10.1175/1520-0442(2000)013<3152:EDHIEA>2.0.CO;2.

——, N. P. Thomas, A. Ruiz-Barradas, and S. J. Weaver, 2017: Striking seasonality in the secular warming of the northern continents: Structure and mechanisms. *J. Climate*, **30**, 6521–6541, https://doi.org/10.1175/JCLI-D-16-0757.1.

Pant, G. B., and K. R. Kumar, 1997: *Climates of South Asia*. John Wiley and Sons, 320 pp.

Parvathi, V., I. Suresh, M. Lengaigne, T. Izumo, and J. Vialard, 2017: Robust projected weakening of winter monsoon winds over the Arabian Sea under climate change. *Geophys. Res. Lett.*, **44**, 9833–9843, https://doi.org/10.1002/2017GL075098.

Quenouille, M. H., 1952: *Associated Measurements*. Academic Press, 242 pp.

Rasmusson, E. M., and T. H. Carpenter, 1983: The relationship between eastern equatorial Pacific SSTs and rainfall over India and Sri Lanka. *Mon. Wea. Rev.*, **111**, 517–528, https://doi.org/10.1175/1520-0493(1983)111<0517:TRBEEP>2.0.CO;2.

Rayner, N. A., D. E. Parker, E. B. Horton, C. K. Folland, L. V. Alexander, D. P. Rowell, E. C. Kent, and A. Kaplan, 2003: Global analyses of sea surface temperature, sea ice, and night marine air temperature since the late nineteenth century. *J. Geophys. Res.*, **108**, 4407, https://doi.org/10.1029/2002JD002670.

Ropelewski, C. F., and M. S. Halpert, 1987: Global and regional scale precipitation patterns associated with the El Niño/Southern Oscillation. *Mon. Wea. Rev.*, **115**, 1606–1626, https://doi.org/10.1175/1520-0493(1987)115<1606:GARSPP>2.0.CO;2.

Santer, B. D., T. M. L. Wigley, J. S. Boyle, D. J. Gaffen, J. J. Hnilo, D. Nychka, D. E. Parker, and K. E. Taylor, 2000: Statistical significance of trends and trend differences in layer-averaged atmospheric temperature time series. *J. Geophys. Res.*, **105**, 7337–7356, https://doi.org/10.1029/1999JD901105.

Schneider, U., A. Becker, P. Finger, A. Meyer-Christoffer, M. Ziese, and B. Rudolf, 2014: GPCC's new land surface precipitation climatology based on quality-controlled in situ data and its role in quantifying the global water cycle. *Theor. Appl. Climatol.*, **115**, 15–40, https://doi.org/10.1007/s00704-013-0860-x.

Sengupta, A., and M. Rajeevan, 2013: Uncertainty quantification and reliability analysis of CMIP5 projections for the Indian summer monsoon. *Curr. Sci.*, **105**, 1692–1703.

Sharmila, S., S. Joseph, A. K. Sahai, S. Abhilash, and R. Chattopadhyay, 2015: Future projection of Indian summer monsoon variability under climate change scenario: An assessment from CMIP5 climate models. *Global Planet. Change*, **124**, 62–78, https://doi.org/10.1016/j.gloplacha.2014.11.004.

Shige, S., Y. Nakano, and M. K. Yamamoto, 2017: Role of orography, diurnal cycle, and intraseasonal oscillation in summer monsoon rainfall over the Western Ghats and Myanmar coast. *J. Climate*, **30**, 9365–9381, https://doi.org/10.1175/JCLI-D-16-0858.1.

Siew, J. H., F. T. Tangang, and L. Juneng, 2014: Evaluation of CMIP5 coupled atmosphere–ocean general circulation models and projection of the Southeast Asian winter monsoon in the 21st century. *Int. J. Climatol.*, **34**, 2872–2884, https://doi.org/10.1002/joc.3880.

Sikka, D. R., 1980: Some aspects of the large scale fluctuations of summer monsoon rainfall over India in relation to fluctuations in the planetary and regional scale circulation parameters. *Proc. Indian Acad. Sci., Earth Planet. Sci.*, **89**, 179–195, https://doi.org/10.1007/BF02913749.

Singh, N., and N. A. Sontakke, 1999: On the variability and prediction of the rainfall in the post-monsoon season over India. *Int. J. Climatol.*, **19**, 309–339, https://rmets.onlinelibrary.wiley.com/doi/10.1002/%28SICI%291097-0088%2819990315%2919%3A3%3C309%3A%3AAID-JOC361%3E3.0.CO%3B2-%23.

Sooraj, K. P., P. Terray, and M. Mujumdar, 2015: Global warming and the weakening of the Asian summer monsoon circulation: Assessments from the CMIP5 models. *Climate Dyn.*, **45**, 233–252, https://doi.org/10.1007/s00382-014-2257-7.

Sridharan, S., and A. Muthuswamy, 1990: Northeast monsoon rainfall in relation to El-Niño, QBO and Atlantic hurricane frequency. *Vayu Mandal*, **20**, 104–111.

Srinivasan, V., and K. Ramamurthy, 1973: Forecasting manual, part IV: Comprehensive articles on selected topics—Northeast monsoon. India Meteorological Department Field Meteorological Unit Rep. IV-18.4, 132 pp., http://imdpune.gov.in/Weather/Forecasting_Mannuals/IMD_IV-18.4.pdf.

Sun, Y., S. C. Clemens, C. Morrill, X. Lin, X. Wang, and Z. An, 2011: Influence of Atlantic meridional overturning circulation on the East Asian winter monsoon. *Nat. Geosci.*, **5**, 46–49, https://doi.org/10.1038/ngeo1326.

Suppiah, R., 1997: Extremes of the Southern Oscillation phenomenon and the rainfall of Sri Lanka. *Int. J. Climatol.*, **17**, 87–101, https://doi.org/10.1002/(SICI)1097-0088(199701)17:1<87::AID-JOC95>3.0.CO;2-X.

Taylor, K. E., R. J. Stouffer, and G. A. Meehl, 2012: An overview of CMIP5 and the experiment design. *Bull. Amer. Meteor. Soc.*, **93**, 485–498, https://doi.org/10.1175/BAMS-D-11-00094.1.

Villafuerte, M. Q., II, J. Matsumoto, I. Akasaka, H. G. Takahashi, H. Kubota, and T. A. Cinco, 2014: Long-term trends and variability of rainfall extremes in the Philippines. *Atmos. Res.*, **137**, 1–13, https://doi.org/10.1016/j.atmosres.2013.09.021.

Walker, G. T., 1923: Correlation in seasonal variations of weather, VIII: A preliminary study of world weather. *Memoirs of the India Meteorological Department*, **24** (4), 75–131.

Wang, B., and LinHo, 2002: Rainy season of the Asian–Pacific summer monsoon. *J. Climate*, **15**, 386–398, https://doi.org/10.1175/1520-0442(2002)015<0386:RSOTAP>2.0.CO;2.

——, and Q. Zhang, 2002: Pacific–East Asian teleconnection. Part II: How the Philippine Sea anomalous anticyclone is established during El Niño development. *J. Climate*, **15**, 3252–3265, https://doi.org/10.1175/1520-0442(2002)015<3252:PEATPI>2.0.CO;2.

Wang, H., and S. He, 2012: Weakening relationship between East Asian winter monsoon and ENSO after mid-1970s. *Chin. Sci. Bull.*, **57**, 3535–3540, https://doi.org/10.1007/s11434-012-5285-x.

Wang, L., W. Chen, and R. Huang, 2008: Interdecadal modulation of PDO on the impact of ENSO on the East Asian winter monsoon. *Geophys. Res. Lett.*, **35**, L20702, https://doi.org/10.1029/2008GL035287.

Watanabe, M., and F.-F. Jin, 2002: Role of Indian Ocean warming in the development of Philippine Sea anticyclone during ENSO. *Geophys. Res. Lett.*, **29**, 1478, https://doi.org/10.1029/2001GL014318.

Wilks, D. S., 2006: *Statistical Methods in the Atmospheric Sciences*. 2nd ed. International Geophysics Series, Vol. 100, Academic Press, 648 pp.

Yatagai, A., K. Kamiguchi, O. Arakawa, A. Hamada, N. Yasutomi, and A. Kitoh, 2012: APHRODITE: Constructing a long-term daily gridded precipitation dataset for Asia based on a dense network of rain gauges. *Bull. Amer. Meteor. Soc.*, **93**, 1401–1415, https://doi.org/10.1175/BAMS-D-11-00122.1.

Zhou, W., X. Wang, T. J. Zhou, C. Li, and J. C. L. Chan, 2007: Interdecadal variability of the relationship between the East Asian winter monsoon and ENSO. *Meteor. Atmos. Phys.*, **98**, 283–293, https://doi.org/10.1007/s00703-007-0263-6.

Zubair, L., and C. F. Ropelewski, 2006: The strengthening relationship between ENSO and northeast monsoon rainfall over Sri Lanka and southern India. *J. Climate*, **19**, 1567–1575, https://doi.org/10.1175/JCLI3670.1.